Pergamon

Materials Research Bulletin 37 (2002) 1797–1813

Materials Research Bulletin

A study on the nuclear and magnetic structure of the double perovskites A_2FeWO_6 (A = Sr, Ba) by neutron powder diffraction and reverse Monte Carlo modeling

A.K. Azad[a,b,*], S.-G. Eriksson[a,b], A. Mellergård[b], S.A. Ivanov[c], J. Eriksen[b], H. Rundlöf[b]

[a]*Department of Inorganic Chemistry, University of Gothenburg, SE-412 96 Göteborg, Sweden*
[b]*Studsvik Neutron Research Laboratory, Uppsala University, SE-611 82 Nyköping, Sweden*
[c]*Karpov Institute of Physical Chemistry, 103064 Moscow, Russia*

(Refereed)
Received 25 March 2002; accepted 25 June 2002

Abstract

Perovskite-type complex metal oxides A_2FeWO_6 (A = Sr, Ba) were prepared by a standard solid state reaction method. Rietveld analysis of neutron powder diffraction (NPD) data at 295 K shows that the Sr_2FeWO_6 (SFW) compound adopts a monoclinic unit cell (space group $P2_1/n$, $a = 5.6480(4)$, $b = 5.6088(4)$, $c = 7.9362(6)$ Å and $\beta = 89.99(2)^\circ$), and the Ba_2FeWO_6 (BFW) compound is tetragonal (space group $I4/m$, $a = 5.7547(4)$, $c = 8.125(1)$ Å). A combination of a reverse Monte Carlo (RMC) technique and Rietveld analysis shows that the low temperature (10 K) magnetic structures of SFW and BFW are antiferromagnetic based on a unit cell related to that of the nuclear structure by a propagation vector, $\boldsymbol{k} = (0\,1/2\,1/2)$. The magnetic moment of iron was found to be $3.86(4)\mu_B$ and $3.49(2)\mu_B$ at 10 K for the Sr- and the Ba-containing compounds, respectively.
© 2002 Elsevier Science Ltd. All rights reserved.

Keywords: A. Magnetic materials; A. Oxides; C. Neutron scattering; D. Crystal structure; D. Magnetic structure

* Corresponding author. Tel.: +46-155-221871; fax: +46-155-263001.
E-mail address: azad@studsvik.uu.se (A.K. Azad).

0025-5408/02/$ – see front matter © 2002 Elsevier Science Ltd. All rights reserved.
PII: S0025-5408(02)00872-3

1. Introduction

Recently research on double perovskites has gained strong interest in particular after the discovery of the metallic and ferrimagnetic characteristic in Sr_2FeMoO_6 and Sr_2FeReO_6 by Kobayashi et al. [1]. The compounds show a critical temperature, T_c around 420 and 400 K, respectively. Since half-metallic ferromagnetism and magnetoresistance (MR) seem to be intimately related to each other, there is an intensive search for half-metallic ferromagnets, which could be candidate materials for the realisation of MR applications. The modification of structural and magnetic properties by changing the A, B′ and/or B″-site cations in $A_2B'B''O_6$ type double perovskites has also gained interest in order to better understand the mechanism of colossal magnetoresistance (CMR) and other unusual physico-chemical properties. Experimental and theoretical efforts have now established a strong coupling of structural, magnetic and electronic property degrees of freedom. Many researchers [1–6] have reported these properties of the double perovskite transition metal oxides, especially for the Fe-based compounds. The structure and physical properties of this type of double perovskites depend strongly on the size and valences of the A, B′ and B″-site cations. Ordering of the B-site cations in the octahedral sublattice [7] plays an important rule on the half-metallic characteristics of the compounds.

SFW was first prepared and characterized as cubic with $a = 7.96$ Å by Blasse [8]. Later Nakagawa et al. [9] reported the compound as tetragonal at room temperature with $a = 7.925(1)$ and $c = 7.985(1)$ Å. Kawanaka et al. [3,4] has found a smaller tetragonal cell with the lattice parameters $a = 5.605$ and $c = 7.947$ Å and the antiferromagnetic (AFM) transition temperature $T_N = 37$ K. The compound BFW was first reported to be a cubic with $a \approx 8.133$ Å [5,10]. All above-mentioned structural studies were done by X-ray powder diffraction (XPD). Recently, we have reported the structure of BFW as tetragonal based on neutron powder diffraction (NPD) [11]. From a structural point of view, our result differs from the ones found in the previous studies. It may be that NPD is a more accurate method to determine the positions of the atoms, especially for light atoms in complex metal oxides, than XPD. We have collected temperature-dependent NPD data in order to extract information concerning the atomic and magnetic structure.

For perovskite systems, the valence of Fe is 3+ in most of the compounds. A new device has already been proposed using organic spin-transition polymers, in which Fe^{2+} ion cause a low-spin–high-spin transition [12]. The double perovskite oxide with iron might be another candidate for spin-transition compounds with Fe^{2+} ions [3,4]. We used a bond valence sum calculation to predict the oxidation-state of Fe and W, which shows mixed valence states for them. We have prepared the compounds in single-phase form and elucidated the nuclear and magnetic structures by using X-ray and temperature-dependent neutron diffraction. The nuclear and magnetic structure is discussed using information from Rietveld analysis and RMC modeling. Structural parameters calculated from the diffraction data are very important in order to understand the physical properties of the compounds since they have a strong correlation. Both the compounds are very interesting to study, because the closely

related compounds, such as Sr_2FeMoO_6 [1,13] and Ba_2FeMoO_6 [2,13], show CMR properties at high temperature.

2. Experimental

2.1. Sample preparation

Polycrystalline samples of A_2FeWO_6 (A = Sr, Ba) were prepared by the conventional ceramic method from stoichiometric amounts of high purity (99.95% or above) starting materials: $SrCO_3$ (Mallinckrodt Chemical Works, USA), $BaCO_3$ (Heraeus, Germany), Fe_2O_3 (Fischer Chemical, USA) and WO_3 (Chemicon, Sweden). The color and formula weight of the starting materials were: $SrCO_3$—white, 147.63 g/mol; $BaCO_3$—white, 197.35 g/mol; Fe_2O_3—red, 159.69 g/mol; and WO_3—light green, 231.85 g/mol. The powders were carefully mixed by ball milling for 6 h, with short breaks between each hour to avoid heating of the sample. Mixed powders were initially calcined in nitrogen at 1223 K for 15 h. Then the powders were reground, pressed into pellets and refired at 1373 K for 48 h, 1623 K for 48 h, and finally at 1693 K for 6 h. Between each sintering step the pellets were ground to a fine powder and new pellets formed before the consecutive heat treatment. All the heat treatments were performed under a controlled nitrogen atmosphere, and heating as well as cooling rates were 4° per minute. Alumina (Al_2O_3) crucibles were used for all heat treatments. In between each sintering step phase purity was checked by XPD. When no impurity phases could be detected the reaction was considered to be complete. XPD patterns were obtained from Guinier film data (Cu $K\alpha_1$ = 1.540598 Å). Silicon (NBS 640b) was used as an internal standard and a computerized line-scanner system [14] for evaluation of the films. Indexing and refinement of the lattice parameters were made with the TREOR90 [15] and PCPIRUM [16] software.

2.2. Neutron diffraction measurements

NPD patterns were obtained at the neutron powder diffractometer at the 50 MW R2 Research Reactor at Studsvik, Sweden. The double monochromator system, consisting of two parallel copper crystals in (2 2 0) mode was aligned to give a wavelength of 1.470(1) Å. The neutron flux at the sample position was approximately 10^6 neutrons cm^{-2} s^{-1}. A powder sample was contained in a thin-walled vanadium cylinder of diameter 8 mm. For the Rietveld analysis, intensity data were collected with a step size of 0.08° over a 2θ range 4–139.92°. The detector bank consisted of 35 ^{3}He detectors with Gd-coated film collimators. A closed cycle refrigerator (CCR) was used for the low temperature measurements.

2.3. Rietveld refinement and RMC modeling

NPD data sets were refined by the Rietveld method by means of the FullProf software [17], using the coherent scattering lengths supplied by the software. Peak

shapes were modeled by a pseudo-Voigt function, with a peak asymmetry correction applied at angles below 45° in 2θ. Background intensities were described by a Chebyshev polynomial with six coefficients. Each structural model was refined to convergence, with the best result selected on the basis of agreement factors and stability of the refinement. Corrections for absorption effects were subsequently carried out in the Rietveld refinements, utilizing the empirical value $\mu_R = 0.1032\ cm^{-1}$ for SFW and $\mu_R = 0.0942\ cm^{-1}$ for BFW.

It is well known that in RMC modeling, a so-called simulated annealing technique can provide information about local correlation and short range ordering [18]. Recently, the technique has been adapted to study both local and long-range order in crystalline materials using powder diffraction data [19]. In the present work, a new RMC program, RMCPOW [20] has been used to model the average magnetic structure.

3. Results and discussions

3.1. Nuclear structure of SFW

The NPD pattern of SFW could be indexed in space group $P2_1/n$ with $a = 5.6480(4)$, $b = 5.6088(4)$ Å, $c = 7.9362(6)$ Å and $\beta = 89.99(2)^\circ$ at 295 K. Other space groups, in particular tetragonal and orthorhombic ones, were tried but the refinement was not satisfactory. A small difference in a and b lattice parameters and a monoclinic β angle close to 90° indicates that the metric of this structure seems to be strongly pseudo-orthorhombic or even pseudo-tetragonal. The real driving force for the monoclinic distortion is the four differently charged cations of Fe (+2 and +3) and W (+5 and +6). The reflection conditions $h\,0\,l$, $h + l = 2n$; $0\,k\,0$, $k = 2n$ *including* $h\,k\,l$, $0\,k\,l$, $h\,k\,0$, $h\,0\,0$ and $0\,0\,l$ *with no condition*, is also indicative of the monoclinic space group $P2_1/n$ (unique axis b). Moreover, the three inequivalent oxygen positions can also be precisely determined by NPD because neutrons are more sensitive to the oxygen positions than X-rays are [21]. In particular, high intensity of $0\,k\,l$: $k = 2n + l$ reflections were indicative of the monoclinic $P2_1/n$ space group [7]. The neutron diffraction data were collected at different temperatures, namely 295, 200, 100, 50, 40, 30, 20 and 10 K. No spurious lines indicative of the presence of a second phase were observed. Unit cell parameters are related to the ideal cubic perovskite as $a \approx \sqrt{2}a_0$, $b \approx \sqrt{2}a_0$, and $c \approx 2a_0$ ($a_0 \approx 3.89$ Å). Twelve positional parameters, six isotropic thermal parameters, 607 reflections and a total of 37 refined parameters converged with $R_p = 3.50\%$, $R_{wp} = 4.62\%$, $R_{Bragg} = 2.08\%$ and $\chi^2 = 1.50$ (Fig. 1). The refined values of the atomic coordinates, thermal parameters and occupancies at 295 K are listed in Table 1. The standard deviations on the coordinates of the oxygen atoms, and consequently on the bond lengths in which they are involved were rather small. No mixing of sites between Fe and W was found during the refinement. The Goldschmidt's tolerance factor (t) [22] was calculated to be $t = 0.961$. The tolerance factor depends on the ionic radii of the constituting

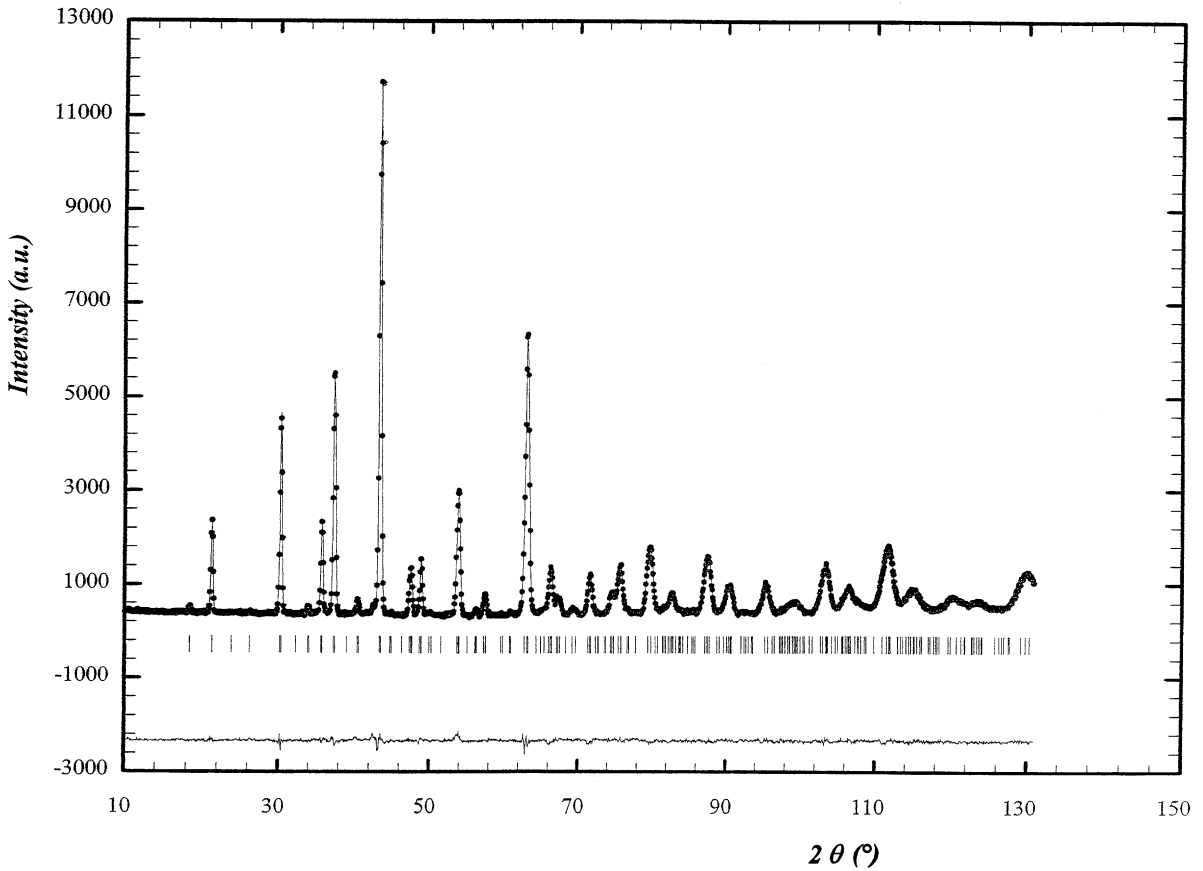

Fig. 1. Observed (circles) and calculated (continuous line) NPD intensity profiles for SFW at room temperature (295 K). The short vertical lines indicate the angular position of the allowed Bragg reflections. At the bottom in each figure the difference plot, $I_{obs} - I_{calc}$, is shown.

Table 1
Refined structural parameters of SFW at 295 K[a]

Atom	Positions	x	y	z	B (Å)^2	Occupancy
Sr	4*e*	−0.0024(9)	−0.0112(6)	0.751(1)	0.63(4)	1.000
Fe	2*d*	0.50	0.00	0.50	0.22(7)	1.000
W	2*b*	0.50	0.00	0.00	0.34(9)	1.000
O(1)	4*e*	0.280(1)	0.261(2)	0.0205(8)	0.80(16)	1.000
O(2)	4*e*	0.241(1)	0.778(1)	0.0309(8)	0.69(13)	1.000
O(3)	4*e*	0.0495(8)	0.507(1)	0.739(1)	0.76(11)	1.000

[a] Crystallographic cell: space group $P2_1/n$, $a = 5.6480(4)$, $b = 5.6088(4)$, $c = 7.9362(6)$ Å and $\beta = 89.99(2)$. $R_p = 3.50\%$, $R_{wp} = 4.62\%$, $R_{Bragg} = 2.17\%$, $\chi^2 = 1.50$.

atoms. Due to the smaller radius of the A-site cations, (Fe, W)O_6 octahedra were tilted in order to optimize the Sr–O bond distances. The FeO_6 and WO_6 octahedra are fully ordered and alternate along the three directions in the crystal structure in such a way that each FeO_6 octahedra is linked to six WO_6 octahedra, and vice versa (see Fig. 2). Several monoclinically distorted perovskites [21,23,24] crystallize in space group $P2_1/n$ and show long-range ordering between the two different cations placed in the B′ and B″ positions. It is a three-tilt system of the kind $a^+b^-b^-$ [25]. The driving force for the B′ and B″ ordering is the size and charge difference between both kinds of cations. It is remarkable that the compound shows an extraordinarily high pseudo-orthorhombic character for all temperatures (295–10 K) as far as unit cell dimensions are concerned. The β angles are close to 90° (see Table 2) which is in analogy with other experiments, for example, $\beta = 89.969(8)^\circ$ in Ca_2FeMoO_6 [23], 90.193(3)° in Ca_2MnWO_6 [21] and 90.4° in Ca_2FeReO_6 [24]. The lattice parameters and *R*-factors at different temperatures are given in Table 2.

Table 2
Main crystallographic and magnetic information for SFW from NPD data at different temperatures

	10 K	20 K	30 K	40 K	100 K	295 K
a_n (Å)	5.6434(5)	5.6438(4)	5.6439(5)	5.6472(4)	5.6459(4)	5.6480(4)
b_n (Å)	5.5856(4)	5.5863(4)	5.5874(4)	5.5928(4)	5.5961(4)	5.6088(4)
c_n (Å)	7.9128(6)	7.9141(6)	7.9158(5)	7.9242(6)	7.9275(5)	7.9362(6)
β (°)	90.033(1)	90.019(3)	90.010(3)	89.981(2)	90.045(3)	89.99(2)
V (Å^3)	249.40(3)	249.51(3)	249.62(3)	250.27(3)	250.43(3)	251.41(3)
a_m (Å)	5.6434(5)	5.6438(4)	5.6439(5)	–	–	–
b_m (Å)	11.1713(4)	11.1727(4)	11.1749(4)	–	–	–
c_m (Å)	15.8257(6)	15.8283(6)	15.8317(5)	–	–	–
μ_B	3.86(4)	3.84(4)	3.19(4)	–	–	–
R_p(%)	4.85	4.70	4.47	3.89	3.67	3.50
R_{wp}(%)	6.72	6.49	5.97	5.28	4.88	4.62
R_B(%)	2.47	2.50	2.18	2.00	1.84	2.08
χ^2	2.32	2.17	1.83	1.55	1.37	1.50
R_{mag}(%)	9.8	8.10	8.4	–	–	–

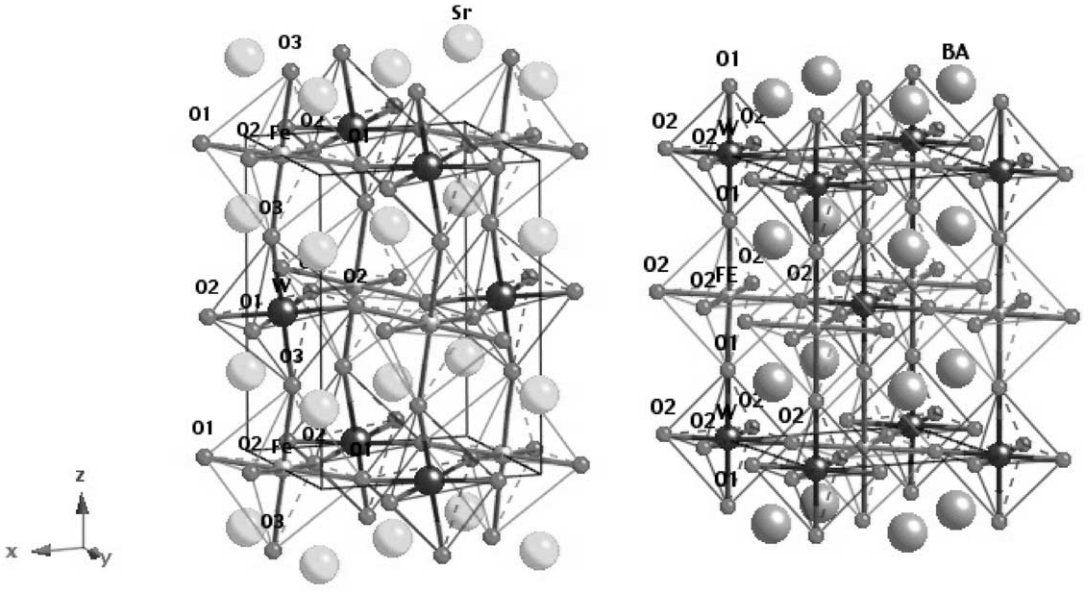

Fig. 2. Comparison of SFW (left side figure) and BFW (right side figure) structure with $P2_1/n$ and $I4/m$ space group symmetry, respectively.

The unit-cell parameters were found to decrease continuously with decreasing temperature, while a discontinuous change can be noticed close to the magnetic phase transition temperature. A small increase at 40 K and a sharp decrease at 30 K is observed in the lattice parameters, which seems to be connected to the paramagnetic to antiferromagnetic phase change. The FeO_6 octahedra (volume = 12.0499(1) Å^3) is significantly larger than the WO_6 octahedra (volume = 9.555(3) Å^3). Due to the $P2_1/n$ symmetry, there is flexibility in the volumes of the individual BO_6 octahedra, thereby permitting a variety of different cation ordering patterns over the B sites. The average B–O bond lengths at 295 K were smaller in comparison to the expected values as calculated from ionic radii sums: ⟨Fe–O⟩, 2.083(8) Å (calculated 2.18 Å); ⟨W–O⟩, 1.928(8) Å (calculated 2.00 Å). It may be the influence of mixed valences on both the Fe and W sites. The combination of the two W cations is not critical for the geometry of the structure ($r_W + 5 = 0.62$ Å and $r_W + 6 = 0.60$ Å) but the main reason for some disagreement may be connected only with Fe ($r_{Fe} + 3 = 0.645$ Å and $r_{Fe} + 2 = 0.78$ Å) [26]. Calculation of bond valence sums (BVS), using Brown's bond valence model [27], from the average bond distances ($d \leq 3.5$ Å) between Fe and O shows that the valence of Fe is +2.33(4), which may indicate a mix of Fe^{2+} and Fe^{3+}. The same type of calculation for W shows that the valence of W is +5.77(8), which may be a mixed valence state of W^{5+} and W^{6+} [3–5]. Average bond distances at 10 K of ⟨Fe–O⟩ (2.082(8) Å) and ⟨W–O⟩ (1.927(9)) Å) do not vary significantly from room temperature data, indicative of the relative stability of the structure. The average Fe–O–W bond angle, which is sensitive to the size of the A cation, is found to be 164.64(6)°. Main bond distances and bond angles are listed in Table 3. It is important to indicate that the average Fe–O and W–O bond lengths remain essentially the same on going from 295 to 10 K. The four planar octahedral bonds for each cation Fe and W initially contract at a rate faster than the average thermal contraction. As the coordinated rotation of the corner linked FeO_6 and WO_6 octahedra grow, this allows the planar Fe–O and W–O bonds to maintain nominally constant lengths in spite of the thermal contraction. This suggests that the average bonds for Fe and W are close to the minimum that can be accommodated in this structure for a given chemical composition. At the same time Sr–O bond lengths are changing noticeable, in some cases dramatically, which is connected to the 12 coordinated position of Sr in the perovskite structure. To illustrate the combined effect of octahedral tilting and cation ordering, Sr–O bond lengths vary irregularly. On the other hand, strong tilting of the octahedra makes the Fe–O–W angles smaller than 180°. A strong tilting of the BO_6-octahedra compared with the ideal cubic structure can be realized by looking at the Fe–O–W bond-angles.

3.2. Magnetic structure of SFW

The 10 K NPD data reveal a number of pure magnetic reflections at low 2θ-angles. These additional reflections could be indexed according to a magnetic unit cell with lattice parameters $a_m = a_n$, $b_m = 2b_n$ and $c_m = 2c_n$, where m and n refer the magnetic and nuclear unit cells, respectively. The initial magnetic model was obtained from

Table 3
Main bond distances (Å) ($d \leq 3.5$ Å) and selected angles (°) for monoclinic SFW determined from NPD data at different temperatures

	10 K	295 K
FeO_6 octahedra		
Fe–O1 (Å) (×2)	2.081(7)	2.081(7)
Fe–O2 (Å) (×2)	2.091(9)	2.084(7)
Fe–O3 (Å) (×2)	2.073(9)	2.085(9)
⟨Fe–O⟩ (Å)	2.082(8)	2.083(8)
Distortion (Δ)[a]	0.00864	0.00192
WO_6 octahedra		
W–O1 (Å) (×2)	1.922(9)	1.925(8)
W–O2 (Å) (×2)	1.929(9)	1.937(7)
W–O3 (Å) (×2)	1.932(9)	1.923(9)
⟨W–O⟩ (Å)	1.927(9)	1.928(8)
Distortion (Δ)	0.005189	0.00726
Fe–O1–W (°) (×2)	149.719(2)	167.13(3)
Fe–O2–W (°) (×2)	147.182(3)	163.43(8)
Fe–O3–W (°) (×2)	147.715(7)	163.38(8)
SrO_{12} polyhedra		
Sr–O1(Å)	3.099(7)	3.076(9)
Sr–O1(Å)	2.798(7)	2.801(9)
Sr–O1(Å)	2.736(7)	2.777(9)
Sr–O1(Å)	2.612(7)	2.611(9)
Sr–O2(Å)	2.775(8)	2.87(1)
Sr–O2(Å)	3.189(8)	3.13(1)
Sr–O2(Å)	2.525(8)	2.56(1)
Sr–O2(Å)	2.765(8)	2.71(1)
Sr–O3(Å)	2.680(6)	2.720(7)
Sr–O3(Å)	2.943(6)	2.922(7)
Sr–O3 (Å)	3.133(6)	3.092(7)
Sr–O3 (Å)	2.516(6)	2.561(7)

[a] Distortion (Δ) in MO_6 octahedra = (longest M–O bond distance − shortest M–O bond distance)/(average M–O bond distance).

RMC modeling of the low temperature (below 40 K) data. RMC modeling with a $2a_n \times 2b_n \times 2c_n$ supercell containing 32 spins, initially with random orientations, was used to obtain the average magnetic structure. About 10 attempts showed unambiguously that the magnetic structure is related to that of the nuclear structure by a propagation vector $\boldsymbol{k} = (0\ 1/2\ 1/2)$; sublattices related by this propagation vector always appeared with close to antiparallel alignment of the magnetic spins. However, the relative orientation of sublattices, not related by this propagation vector, show considerable variation. Presumably due to lack of statistics and resolution, final models, with nearly the same agreement of calculated and experimental data, ranged from full 90° canting to an almost collinear arrangement of sublattices. For the final refinement we constrained spins to be collinear and used a multiphase Rietveld analysis. The agreement between the observed and the calculated diffractogram was

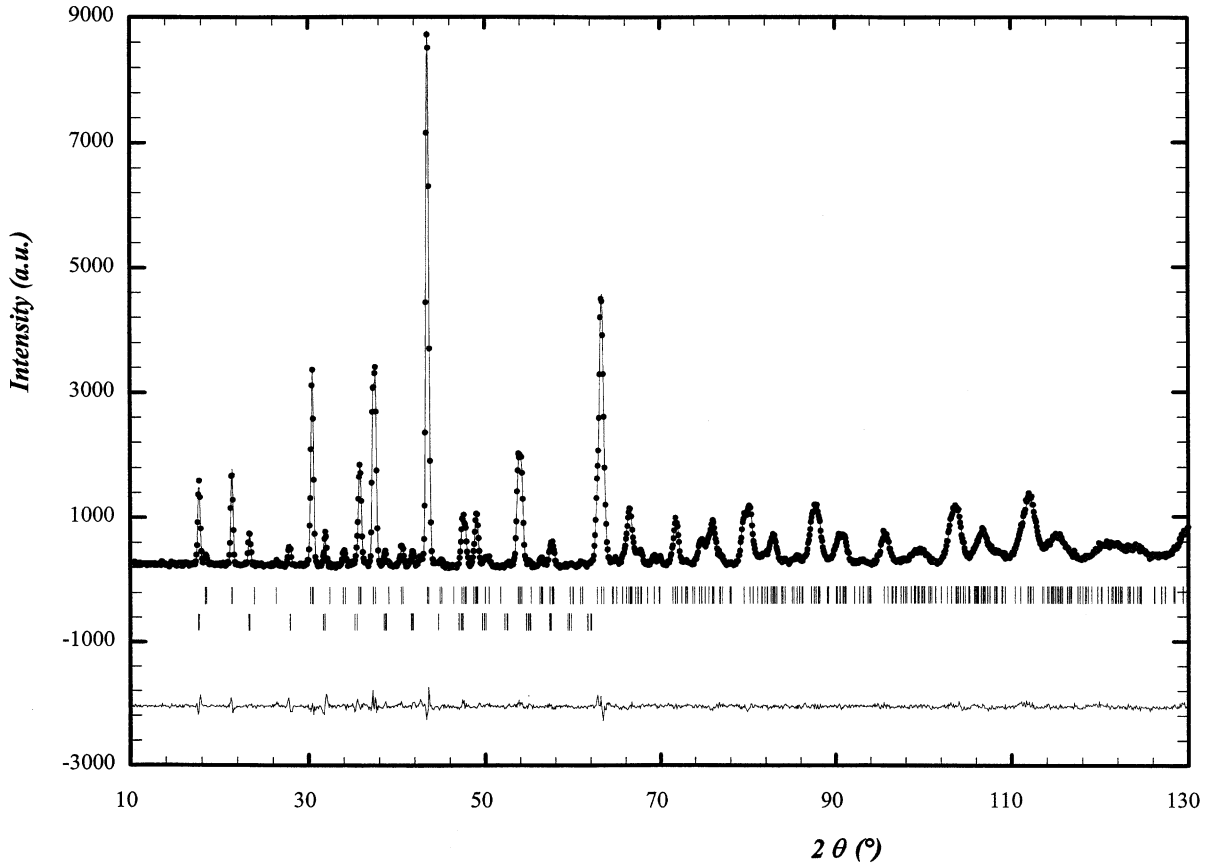

Fig. 3. Observed (circles) and calculated (continuous line) NPD intensity profiles for SFW at 10 K. The short vertical lines indicate the angular position of the allowed Bragg reflections. At the bottom in each figure the difference plot, $I_{obs.} - I_{calc.}$, is shown.

very good, according to the analysis by the Fullprof software. The magnetic structure was refined in space group $P-1$ as an independent phase for which only the iron sites were defined and only magnetic scattering was calculated. The different structures were modelled with magnetic moments at the Fe positions. The model was refined with reflections in the 2θ-range 4–60°. The final result of the refinement at 10 K is shown in Fig. 3. After the full refinement of the profile, including the magnitude of the magnetic moment and its orientation, a best discrepancy factor R_{mag} of 9.8% was reached for an antiferromagnetic (AF) model. The magnetic moments increase with decreasing temperature and a total magnetic moment of $3.19(4)\mu_B$, $3.84(4)\mu_B$ and $3.86(4)\mu_B$ was obtained at 30, 20 and 10 K, respectively. The direction of the moments were $M_x = -3.63(6)$, $M_y = 0.39(5)$, $M_z = 1.24(9)$ at 10 K. The Néel temperature is in between 30 and 40 K. Fig. 4 shows the orientation of the magnetic moments in the unit cell. The magnetic structure can be described as alternating set of (0 1 1) ferromagnetic planes coupled antiferromagnetically (+−+−) (see Fig. 4) with the spins nearly aligned with the propagation vector.

3.3. Nuclear structure of BFW

The neutron diffraction data were collected at different temperatures (the same as for SFW). The reflection condition allows us to propose the tetragonal space group *I*4/*m* (no. 87). The Glazer notation [25] of the distortion is $a^{\circ}a^{\circ}c^{-}$ (one tilt system), which can illustrate the combined effect of cation ordering and octahedral tilting. According to this tilting system, the octahedra are not tilted from each other, as in the ideal cubic perovskite structure, when viewed along the [1 1 0] direction. They are tilted alternatively along the [0 0 1] direction (Fig. 2).

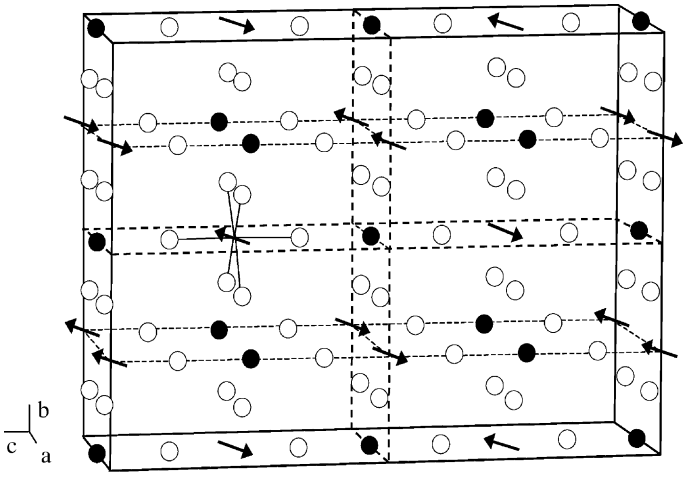

Fig. 4. The orientation of magnetic moments in SFW. The arrows indicate the direction of the magnetic moments at the Fe sites. Filled circles are W and open circles are O. Since magnetic orientation is same in both samples, one figure is given.

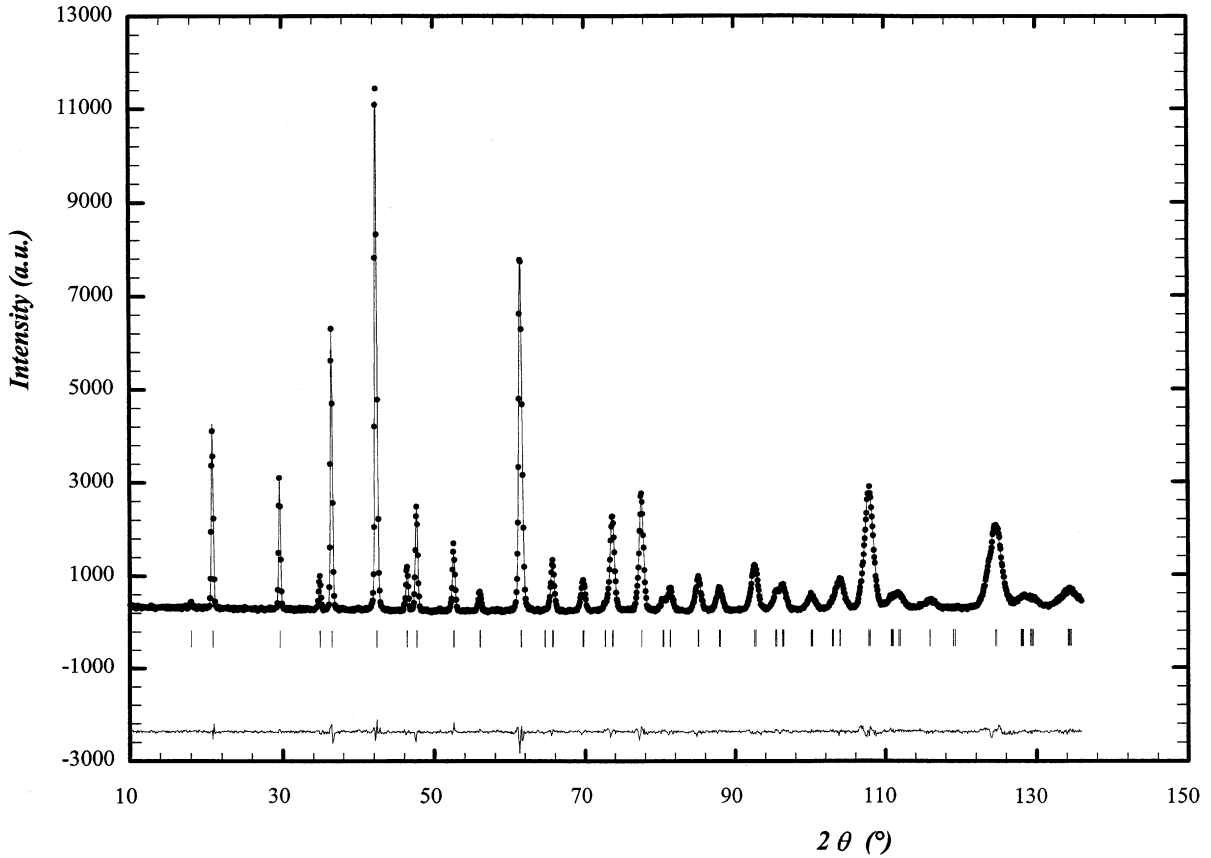

Fig. 5. Observed (circles) and calculated (continuous line) NPD intensity profiles for BFW at room temperature (295 K). The short vertical lines indicate the angular position of the allowed Bragg reflections. At the bottom in each figure the difference plot, $I_{obs} - I_{calc}$, is shown.

The unit cell parameters are related to that of ideal cubic perovskite as $a \approx \sqrt{2}a_p$, $b \approx \sqrt{2}a_p$, $a \approx 2a_p$ ($a_p \approx 3.89$ Å). The 25 variable parameters including lattice parameters, positional parameters, isotropic thermal parameters and 157 reflections resulted in the following R-factors: $R_p = 4.18\%$, $R_{wp} = 5.38\%$, $R_{Bragg} = 1.93\%$, $\chi^2 = 1.80$. The observed and calculated patterns, differences and the peak positions for the neutron diffraction pattern at room temperature are shown in Fig. 5. No structural phase transition takes place between 295 and 10 K, only a general compression of the structure can be noticed. A small discontinuity was observed at 20 K, which might be closely connected to magnetic phase transition. Structure parameters, interatomic distances and R-factors obtained from the analysis are summarized in Table 4. The Wyckoff positions were for Fe 2*b*, for W 2*a*, for Ba 4*d* and for O 4*e* and 8*h*, which gives an ordered perovskite structure of the so-called elpasolite type. Fe and W are found to occupy alternate B sites. The volume of the FeO_6 and WO_6 octahedra was calculated to be 12.9521(4) and 9.6396(8) Å^3.

Table 4
Main crystallographic and magnetic information for BFW (space group *I*4/*m*) from NPD data at different temperatures

	10 K	20 K	30 K	40 K	100 K	295 K
$a_n = b_n$ (Å)	5.7446(5)	5.7448(4)	5.7448(5)	5.7452(4)	5.7457(5)	5.7547(4)
c_n (Å)	8.1099(9)	8.1066(9)	8.111(1)	8.111(1)	8.114(1)	8.125(1)
V (Å^3)	267.63(5)	267.45(6)	267.67(5)	267.73(5)	267.88(6)	269.06(5)
a_m (Å)	5.7446(5)	5.7452(4)	–	–	–	–
b_m (Å)	11.489(5)	11.4904(4)	–	–	–	–
c_m (Å)	16.2199(9)	16.218(1)	–	–	–	–
Ba in 4*d*(0 1/2 1/4)						
B (Å^2)	0.04(5)	0.07(5)	0.08(3)	0.09(2)	0.14(2)	0.31(3)
Fe in 2*b*(0 0 1/2)						
B (Å^2)	0.09(9)	0.20(9)	0.13(6)	0.12(2)	0.13(5)	0.28(6)
μ_B	3.49(2)	1.88(5)	–	–	–	–
W in 2*a*(0 0 0)						
B (Å^2)	0.3(2)	0.3(2)	0.3(1)	0.2(1)	0.2(1)	0.3(1)
O1 in 4*e*(0 0 *z*)						
z	0.241(3)	0.240(1)	0.236(1)	0.238(2)	0.234(1)	0.237(2)
B (Å^2)	0.4(3)	0.8(3)	0.4(2)	0.8(2)	0.3(2)	0.9(3)
O2 in 8(*x y* 0)						
x	0.239(3)	0.238(4)	0.238(3)	0.239(3)	0.239(9)	0.235(2)
y	0.235(3)	0.238(4)	0.240(2)	0.236(3)	0.240(2)	0.241(1)
B (Å^2)	0.2(2)	0.05(1)	0.3(1)	0.3(1)	0.4(1)	0.5(1)
Reliability factors						
R_p (%)	4.50	4.52	4.36	4.28	4.22	4.18
R_{wp} (%)	5.94	5.89	5.76	5.56	5.56	5.38
R_B (%)	1.13	2.02	1.49	1.42	1.63	1.93
χ^2	1.59	1.57	1.64	1.53	1.54	1.80
R_{mag} (%)	7.33	9.01	–	–	–	–

Table 5
Main bond distances (Å) ($d \leq 3.5$ Å) for BFW determined from NPD data at 10 and 295 K

	10 K	295 K
FeO_6 octahedra		
Fe–O1 (Å) (×2)	2.099(3)	2.132(4)
Fe–O2 (Å) (×4)	2.135(3)	2.135(3)
⟨Fe–O⟩ (Å)	2.117(6)	2.1335(7)
Distortion (Δ)	0.0170	0.0014
WO_6 octahedra		
W–O1 (Å) (×2)	1.956(7)	1.931(8)
W–O2 (Å) (×4)	1.927(7)	1.935(8)
⟨W–O⟩ (Å)	1.9415(7)	1.933(8)
Distortion (Δ)	0.01493	0.002069
Fe–O1–W (°)	180.00	180.00
Fe–O2–W (°)	179.08(4)	177.92(5)
BaO_{12} polyhedra		
Ba–O1(Å) (×4)	2.8732(4)	2.8791(5)
Ba–O2(Å) (×4)	2.880(5)	2.903(6)
Ba–O2(Å) (×4)	2.863(5)	2.851(6)

The FeO_6 and WO_6 octahedra are ordered and alternate along the three directions in the crystal structure in such a way that each FeO_6 octahedra is linked to six WO_6 octahedra and vice versa (see Fig. 2) as in SFW. The main bond distances ($d \leq 3.5$ Å) at 295 and 10 K are given in Table 5. According to the ionic radius (coordination number taken into account) of Ba^{2+} ($r = 1.61$ Å), Fe^{2+} ($r = 0.78$ Å), W^{6+} ($r = 0.60$ Å) and O^{2-} ($r = 1.40$ Å) [26], the tolerance factor was calculated to be $t \approx 1.00$. Bond valence calculation from our observed data shows that the charge distributions of Fe and W cations in BFW are also close to Fe^{2+} (calculated 2.04) and W^{6+} (calculated 5.75), respectively.

3.4. Magnetic structure of BFW

Temperature-dependent NPD data shows that the appearance of extra peaks at 20 K and the intensity of these peaks were increased about 50% at 10 K. These extra peaks can be indexed by a magnetic unit cell with lattice parameters $a_m = a_n$, $b_m = 2b_n$ and $c_m = 2c_n$, where m and n refer to the magnetic and nuclear unit cells, respectively. The refinement procedure was the same as described for SFW. The magnetic structure is related to that of the nuclear structure by a propagation vector (0 1/2 1/2). The magnetic structure was refined in space group $P-1$ as an independent phase for which the orientations of the Fe^{2+} magnetic moments were coupled in sublattices. The observed, calculated and difference patterns, and peak positions at 10 K is shown in Fig. 6. This model can be described as alternating set of (0 1 1) ferromagnetic planes coupled antiferromagnetically (+−+−) (see Fig. 4). After full refinement of the profile, including the magnitude of the magnetic moment and its orientation, a final discrepancy factor R_{mag} of 8.83% was reached. A total magnetic moment of

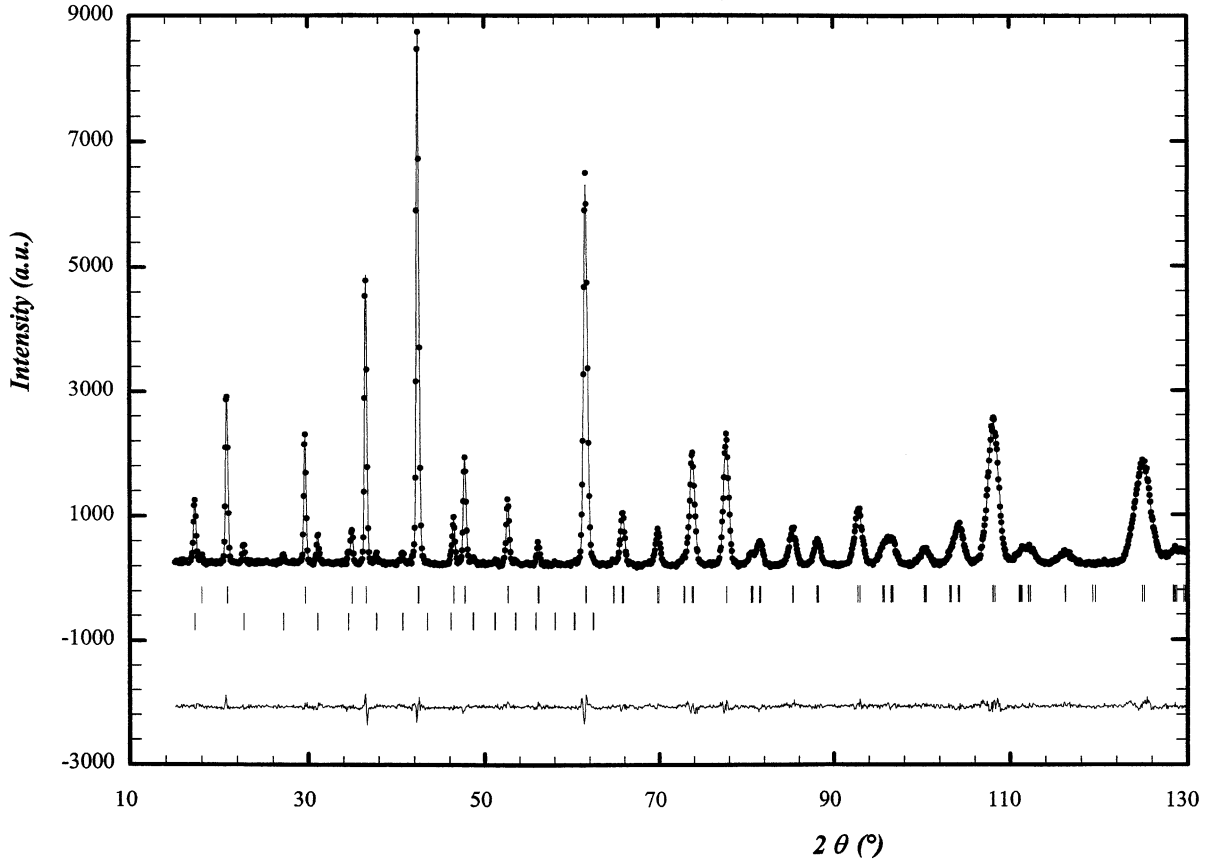

Fig. 6. Observed (circles) and calculated (continuous line) NPD intensity profiles for BFW at 10 K. The short vertical lines indicate the angular position of the allowed Bragg reflections. At the bottom in each figure the difference plot, $I_{obs} - I_{calc}$, is shown.

1.88(4)μ_B and 3.49(2)μ_B was obtained at 20 and 10 K, respectively. At 10 K, the direction of magnetic moments were $M_x = -0.61(3), M_y = 2.87(6), M_z = -1.77(9)$. Since the intensity of the magnetic peaks at 30 K are zero, the antiferromagnetic transition temperature takes place between 20 and 30 K.

4. Conclusions

In summary, we have presented a detailed crystallographic and magnetic characterization of the double perovskites A_2FeWO_6 (A = Sr, Ba) by means of temperature-dependent neutron diffraction measurements. Our results are consistent with an antiferromagnetic coupling of the magnetic moments caused by the unpaired electrons at the iron sites in both of the compounds at low temperature. No evidence of significant mis-site cation disorder was found during refinements of neutron diffraction data. There was no significant evidence of any off-stoichiometry effect either. The symmetry was increased with the increase of A-site ionic radius. The magnetic moments obtained from Rietveld refinement of 10 K data were 3.86(4)μ_B and 3.49(2)μ_B for SFW and BFW, respectively. These moments decreased with increased temperature below the Néel temperature.

Acknowledgments

We would like to acknowledge the financial support from the Swedish Natural Science Research Council (NFR), The Royal Academy of Sciences and the Swedish Foundation of Strategic Research (SSF). A.K. Azad gratefully acknowledges the financial support from the ''Research, development and training project of the Bangladesh Atomic Energy Commission.''

References

[1] K.-I. Kobayashi, T. Kimura, H. Sawada, K. Terakura, Y. Tokura, Nature 395 (1998) 677; K.-I. Kobayashi, T. Kimura, H. Sawada, K. Terakura, Y. Tokura, Phys. Rev. B 59 (1999) 11159.
[2] A. Maignan, B. Raveau, C. Martin, M. Hervieu, J. Solid State Chem. 144 (1999) 224.
[3] H. Kawanaka, I. Hase, S. Toyama, Y. Nishihara, Phys. B 284/288 (2000) 1428.
[4] H. Kawanaka, I. Hase, S. Toyama, Y. Nishihara, Phys. B 281/282 (2000) 518.
[5] T. Nakagawa, S. Nomura, J. Phys. Soc. Japan 29 (1970) 746.
[6] C. Ritter, M.R. Ibarra, L. Morellon, J. Blasco, J. Garcia, J.M. De Teresa, J. Phys.: Condens. Matter 12 (2000) 8295.
[7] M.T. Anderson, K.B. Greenwood, G.A. Taylor, K.R. Poeppelmeier, Prog. Solid State Chem. 22 (1993) 197.
[8] G. Blasse, J. Inorg. Nucl. Chem. 27 (1965) 993.
[9] T. Nakagawa, K. Yoshikawa, S. Nomura, J. Phys. Soc. Japan 27 (1969) 880.
[10] J. Fresia, L. Katz, R. Ward, J. Am. Chem. Soc. 81 (1959) 4783.
[11] A.K. Azad, A. Mellergård, S.-G. Eriksson, S.A. Ivanov, J. Eriksen, H. Rundlöf, Appl. Phys. A 75 (2002) 1–3, DOI; 10.1007/5003390101151.

[12] O. Kahn, C.J. Martines, Science 279 (1998) 44.
[13] R.P. Boges, R.M. Thomas, C. Cullinan, J.M.D. Coey, R. Suryanarayanan, L. Ben-Dor, L. Pinsard-Gaudart, A. Revcolevschi, J. Phys.: Condens. Matter 11 (1999) L445.
[14] K.E. Johansson, T. Palm, P.-E. Werner, J. Phys. E. Sci. Instrum. 13 (1980) 1289.
[15] P.-E. Werner, Z. Kristallogr. 120 (1964) 375.
[16] P.-E. Werner, Ark. Kemi 31 (1969) 513.
[17] J. Rodrigues-Carvajal, Phys. B 192 (1993) 55.
[18] R.L. McGreevy, Nucl. Instrum. Meth. A 354 (1995) 1.
[19] A. Mellergård, R.L. McGreevy, S.-G. Eriksson, J. Phys.: Condens. Matter 12 (2000) 4975.
[20] A. Mellergård, R.L. McGreevy, Acta Cryst. A 55 (1999) 783.
[21] A.K. Azad, S.A. Ivanov, S.-G. Eriksson, J. Eriksen, H. Rundlöf, R. Mathieu, P. Svedlindh, Mater. Res. Bull. 36 (2001) 2485.
[22] V.M. Goldschmidt, Str. Nor. Vidensk-Akad. Oslo 1 (1926) 1.
[23] J.A. Alonso, M.T. Casais, M.J. Martinez-Lope, J.L. Martinez, P. Velasco, A. Munoz, M.T. Fernández-Diaz, Chem. Mater 12 (2000) 161.
[24] W. Prellier, V. Smolyaninova, A. Biswas, C. Galley, R.L. Greene, K. Ramesha, J. Gopalakrishnan, J. Phys.: Condens. Matter 12 (2000) 965.
[25] A.M. Glazer, Acta Crystallogr. B 28 (1972) 3384.
[26] R.D. Shannon, Acta Crystallogr. A 32 (1976) 751.
[27] I.D. Brown, in: M. O'Keefe, A. Navrotsky (Eds.), Structure and Bonding in Crystals, Vol. 2, Academic Press, New York, 1981, pp. 1–30.